CHARACTERIZATION AND SIMULATION OF CU2ZNSNS4 ABSORBER LAYERS FABRICATED BY SEQUENTIAL DC MAGNETRON SPUTTERING AND RAPID THERMAL PROCESSING

Maria Zhukova[1]*, Ratan Kotipalli[1], Louise Samain[2], Lionel Fourdrinier[2], Denis Flandre[1]
[1] ICTEAM, UC Louvain, Place du Levant 3, 1348, Louvain-la-Neuve, Belgium
[2] CRM Group, Allée de l'Innovation 1, B57- Quartier Polytech 3, 4000 Liège, Belgium
Phone: +32 (0) 10 47 26 09, e-mail: maria.zhukova@uclouvain.be

ABSTRACT : The thin-film Cu_2ZnSnS_4 (CZTS) solar cell technology is seen as a sustainable and low cost alternative to the CIGS technology. However mastering the CZTS formation is not evident. In particular, the deposition parameters of each layer in the metallic precursor impact on properties of these layers and could influence the final Cu_2ZnSnS_4 (CZTS) absorber quality. To verify and quantify these influences, two kinds of samples with low-density and high-density precursors have been fabricated by sequential DC magnetron sputtering and finalized into CZTS by Rapid Thermal Processing (RTP) with presence of elemental sulfur. In addition to optical and material characterizations, Hall measurements were carried out for estimation of the carrier concentration, mobility and conductivity of fabricated layers. Finally, SCAPS simulations have been run to predict the cell efficiency and compare with experiments. This study demonstrates that appropriate optoelectrical properties : $E_G \sim 1.5\text{-}1.6$ eV, $\alpha > 2 - 3\times10^4$ cm^{-1}, $\mu_h \sim 25\text{-}30$ cm^{2}V^{-1}s^{-1}, $p \sim 5\text{-}6\times10^{15}$ cm^{-3}, rather than absorber composition and morphology, are the success criteria for obtaining high-efficiency (~ 10 %) CZTS-based devices. Therefore, a monitoring of the optoelectrical parameters during the fabrication steps may be particularly relevant to assess the absorber quality in industrial process.
Keywords: Thin film solar cell, CZTS, Sputtering, Rapid Thermal Processing, Optoelectrical properties, Simulation

1 INTRODUCTION

To date, the highest PV efficiency achieved by pure sulfide kesterite Cu_2ZnSnS_4 (CZTS) solar cells fabricated by co-sputtering and annealing of the precursors is of 9.2 % [1], while it still lags behind at 5.2 % only for sequential sputtering of metallic layers in precursor stack [2]. However, this two-step method is considered as the most environment-friendly and industrially viable for large-scale production with future application towards roll-to-roll process on flexible substrates [3]. To try to understand the material and process limitations, many works concerning the characterization and optimization of the CZTS absorber have been focused on structural and optical material properties [4] as well as complete cells [5, 6] but did not report all electronic parameters, i.e., p-type carrier concentration (p) and mobility (μ_h), or discussed the values actually needed for high-efficiency cells.

The aim of the present work is to establish, for the first time, to our best knowledge, a correlation between the process parameters using sequential DC magnetron sputtering and the material and electrical properties of the obtained CZTS layers. The relevance of the results for realizing high-efficiency cells is assessed by means of SCAPS simulations.

2 EXPERIMENTAL DETAILS

2.1 Film deposition, sulfurization and cell finalization

CZTS layers have been fabricated by sequential DC magnetron sputtering (in a Kurt J. Lesker vacuum system) of multilayer precursors from pure (99.99%), 76.2 mm diameter copper (Cu), tin (Sn) and zinc (Zn) targets. The sputtering deposition was carried out at room temperature using Ar as the working gas. The base pressure of the sputtering chamber was about 10^{-6} Torr and 2 mm soda lime glass substrates were used and placed at 110 mm distance to target. This fabrication step allows to adjust composition in metallic precursor easily by deposition time variation. The deposited thicknesses and masses have been controlled by systematic measurements using a Dektak 150 stylus profiler and a 5-decimals microbalance (METTLER AE 200) respectively. For calibration samples, the deposited mass has been double controlled by ICP measurements. Then, recrystallization into polycrystalline thin film and sulfur (S) incorporation are achieved by simultaneous rapid thermal process (RTP) and sulfurization. The sputtering technique also allows for obtaining deposited films with a composition close to that of the source matter. But the deposition parameters impact a lot on the density and adhesion. Two different deposition conditions (Table I) were chosen to obtain low-density (L) and high-density (H) Sn and Zn layers while Cu layer density was kept almost constant close to bulk density. The resulting volume densities, ρ(Cu), ρ(Zn) and ρ(Sn), have been calculated from the measurements of deposited masses Δm (with $\pm$ 0.1 mg precision) and thicknesses (with $\pm$50 nm precision) of thin layers. The densities ρ for Zn and Sn layers have been estimated as one third of the bulk densities for L precursors and one half of the bulk densities for H ones. These results have been achieved by varying mainly the current and working pressure. For each deposition condition, three different metallic stacks were tested with different composition ratios (Table II). The usual way to fix the ratios of the elements in the precursor is to fix their effective thickness, but depending on the deposition parameters, the same deposited mass will result in denser (thinner) or less dense (thicker) layer. So, in the present work, the ratios of precursors are calculated from the extracted densities per unit area $\rho^S = \Delta m/S$ (g/m²), where S is the 40 × 40 mm² sample area.

All precursors were sulfurized under the same conditions in an AS-ONE 100 RTP system. The samples were placed inside of a graphite box together with ~100 mg of S, ~10 mg of Sn powder and ~30 mg of SnS. This box was placed in the reactor and heated up to 550°C at a rate of 3°C/s and kept at this temperature during 5 minutes. This rapid heating is insured by halogen lamps in Ar atmosphere at a pressure of 0.9 bar. Finally the samples were left to cool down inside the reactor to room temperature, at cooling rate estimated as ~24°C/min. The RTP choice for sulfurization step was done as it showed

good results in terms of limiting secondary phase generation and SnS losses [7] as well it is favourable at industrial conditions.

Some preliminary cells were completed in conventional structure SLG/Mo/CZTS/CdS/iZnO/AZO based on the obtained CZTS films. The Mo back contact of about 0.8 µm thick was prepared by DC magnetron sputtering. CdS layer of 40 nm thick was prepared by chemical bath deposition at 60°C during 9 minutes. I-ZnO and AZO were prepared by RF and DC magnetron sputtering with thickness about 100 nm and 350 nm, respectively. The resulted sheet resistance of i- ZnO/AZO measured on calibration samples was about 100 Ohm/sq. Al grids of ~1 µm thick were deposited by evaporation.

Table I: Deposition conditions for Low-density and High-density precursors: $\rho^{bulk}(Cu)$, $\rho^{bulk}(Zn)$ and $\rho^{bulk}(Sn)$ denote the mass densities for copper, zinc and tin solid elements : 8920 kg.m^{-3}; 7140 kg.m^{-3} and 7310 kg.m^{-3} respectively [8]

	Low-density precursors: $\rho(Cu) \sim \rho^{bulk}(Cu)$ $\rho(Sn) \sim \rho^{bulk}(Sn)/3$ $\rho(Zn) \sim \rho^{bulk}(Zn)/3$			High-density precursors: $\rho(Cu) \sim \rho^{bulk}(Cu)$ $\rho(Sn) \sim \rho^{bulk}(Sn)/2$ $\rho(Zn) \sim \rho^{bulk}(Zn)/2$		
Parameters	Power, W	Current, A	Pressure, mTorr	Power, W	Current, A	Pressure, mTorr
copper layer	230	0.82	3.21	150	0.42	2.44
zinc layer	131	0.62	4.61	150	0.34	2.44
tin layer	50	0.20	2.99	50	0.13	2.44

Table II: Relative mass ratios of the six different stacks compared to target [9] ratios in brackets

Samples names	L1	L2	L3	H1	H2	H3
Stack order	Cu/Zn/Sn	Cu/Zn/Sn	Cu/Zn/Sn	Cu/Sn/Zn	Cu/Sn/Cu/Zn	Cu/Sn/Cu/Zn
Density per unit area, g/m²	0.85/0.98/1.43	1.35/1.29/0.92	1.63/1.22/1.81	1.60/1.32/1.99	-/1.80/1.60/1.20	-/1.5/1.63/1.22
Cu/(Sn+Zn) (0.75)	0.62	0.95	1.96	0.68	0.73	0.76
Zn/Sn (1.22)	1.36	1.36	1.30	1.24	1.22	1.22
Cu/Sn (1.68)	1.47	2.24	2.54	1.51	1.61	1.68
Cu/Zn (1.37)	1.08	1.65	1.96	1.22	1.31	1.37

2.2 Film and cell characterization, simulation

For finished CZTS layers, the normal-incident transmittance spectra in the 250-2500 nm wavelength range were recorded using Perkin Elmer Lambda 950 UV-vis spectrometer, equipped with an integration sphere. These data were used to evaluate absorption coefficients and optical bandgaps for the different samples. Hall measurements were done with Ecopia HMS-3000 system. This equipment uses the Van der Pauw configuration and 0.55 T magnetic field for measuring the resistivity, carrier concentration and mobility in fabricated CZTS layers.

X-Ray Diffraction (XRD) measurements, using CuKα radiation with an acceleration voltage of 30 kV, 30 mA and Bragg-Brentano geometry, were performed for structural examination of the CZTS thin films. The XRD data were collected from 20° to 80° of 2Theta using a high-resolution Bruker D8 Advance diffractometer. Additional Raman spectroscopy measurements were performed using a LabRAM HR 800 instrument from Horiba Scientific. A 514 nm wavelength laser and a 2400 grooves/mm grating were used. The laser was focused onto the sample using a 100x objective with N.A.= 0.95 (spot size ~1 µm).

The surface morphology of the thin films was characterized by Field Emission Scanning Electron Microscope (SEM, ULTRA55). The composition ratio of the thin films was analyzed by Energy Dispersive X-Ray (EDX) spectroscopy integrated with SEM.

For cell measurements, a Newport Oriel IV Solar simulator equipped with a Xenon lamp was used. IV curves were recorded under AM 1.5 illumination and irradiance of 1000 W/m^2 was calibrated with a reference silicon cell. The sample temperature was not regulated.

Using the CZTS measured optical and electrical parameters the SCAPS [10] simulations have been performed to assess the influence of these parameters and predict perspectives for solar cell performance.

3 RESULTS AND DISCUSSION

3.1. Material CZTS layers characterization

XRD spectra normalized to their maximum peak for all 6 absorber layers (Fig. 1) show the presence of the CZTS phase. For samples L2 and H2, a buckling can be mentioned, which is most probably related to the presence of amorphous phase in the layers at range of 40-50 deg. The bucking at the beginning (~20 deg.) of the scan corresponds more to the amorphous state of the substrate.

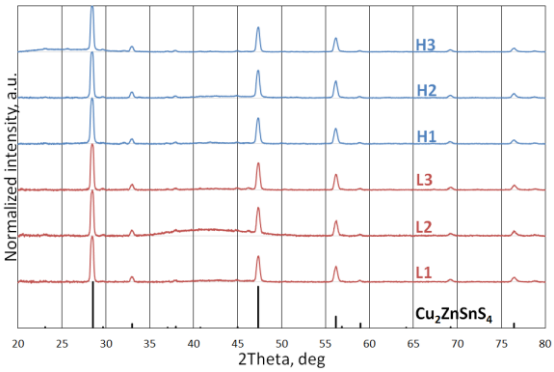

Figure 1: XRD spectra for our 6 CZTS samples and expected peak positions from PDF 26-0575 database

Raman spectra (Fig. 2) confirm the presence of the kesterite CZTS phase with peaks at 288 cm^{-1}, 336 cm^{-1} and 369 cm^{-1} frequencies [11]. But some indications on peaks from the ZnS, SnS or $Cu_{x-1}SnS_x$ (CTS) phases can also be outlined [11]. Samples L2 and L3 feature additional peaks at 468 cm^{-1} corresponding to $Cu_{2-x}S$ phase [11]. This indicates the coexistence of different phases or/and composition and crystal orientation variation. No clear trend with the deposition conditions was identified till now.

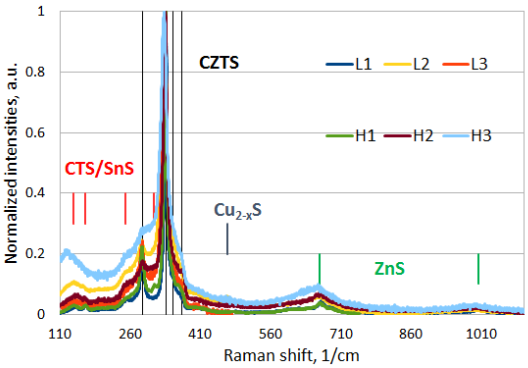

Figure 2: Raman spectra for our six CZTS layers versus expected peak positions for different alloys

After sulfurization, all layers appear grey and present some roughness. Fig. 3 shows top and cross section views of the six layers under discussion. Samples of L-series have inhomogeneous surface morphology. Clearly two different regions can be distinguished: compact islands with round-shaped grains of different sizes (0.2-2 µm) or regions composed of fine grains with round shape (size of tens of nanometres). Sample L1 has additional infusion of rice-shape grain region. Based on literature, we attributed the rice-shaped morphology to the SnS phase and fine-grains region to ZnS phases [11]. The EDX composition analysis confirms these hypotheses by too high concentration in Sn (16 at.%) and S (28 at.%) for SnS and Zn (18 at.%) and S (28 at%) for ZnS regions. This should be due to initial ratios in precursors of these samples. The compact region is mostly present in all samples and was taken into account for composition analysis at 1000 times magnification over 50 measured points (Fig. 4).

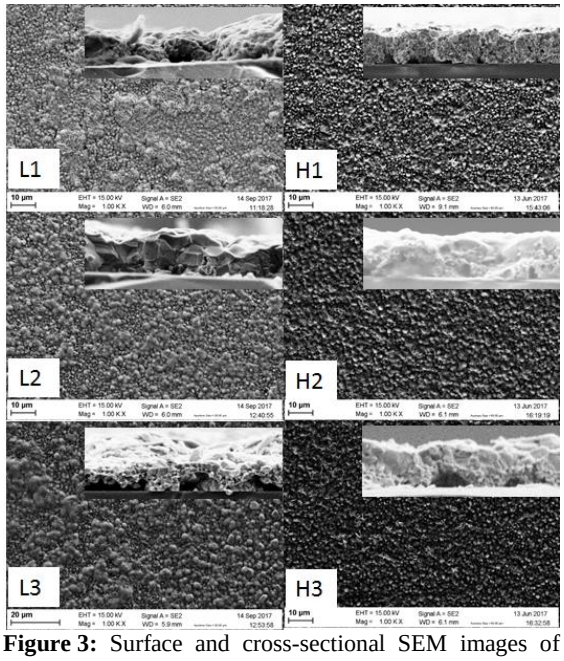

Figure 3: Surface and cross-sectional SEM images of CZTS layers

All films of H series showed homogeneous morphology of compact fine grains. But still two different regions in composition can be outlined. The overall composition is slightly tin-rich and zinc-poor, which is correlated with compositions in precursors.

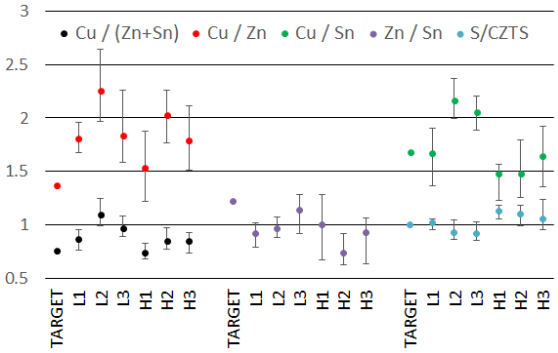

Figure 4: Composition ratios with minimum and maximum values as error bars for all samples compared to target ratios from [9]

In cross-section views, some voids over thickness can be observed for all samples. This could be due to poor adhesion of absorber with substrate. The average thickness is ~1.5 µm for samples of L series and ~2 µm for H samples.

3.2 Optoelectrical properties of CZTS layers

All samples showed relatively good (lower than 60 %) transmittance for all wavelengths, and samples L2 and L3 even lower than 40% (Fig. 5). This can be correlated with the presence of the opaque sub-metallic CuS phase, according to the phase analyses.

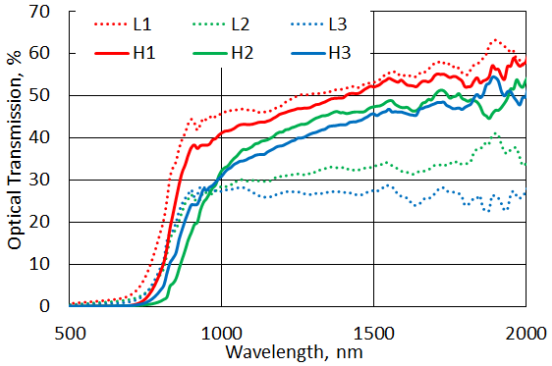

Figure 5: UV-vis transmission results as collected by spectrometer

Bandgaps E_G and averages of absorption coefficient in 250-2000 nm wavelength range are calculated from Fig. 6 and summarized in Table III. They appear in good correlation with literature, i.e. about 1.45 eV and 10^4 respectively [12].

Table III: Band gap, absorption coefficient and Hall measurement results for our 6 CZTS absorber layers

	E_G eV	α 10^4 cm^{-1}	p cm^{-3}	µ cm^2 $V^{-1}s^{-1}$	ρ Ω.cm
L1	1.53	1.73	1.1×10^{13}	14.04	8.5×10^{4}
L2	1.43	2.02	2.0×10^{20}	0.19	9.8×10^{-1}
L3	1.49	2.17	5.0×10^{19}	1.04	5.4×10^{-1}
H1	1.58	2.17	8.8×10^{13}	26.41	1.4×10^{4}
H2	1.39	2.26	7.8×10^{15}	5.52	7.6×10^{2}
H3	1.49	2.16	1.8×10^{16}	0.33	2.1×10^{3}

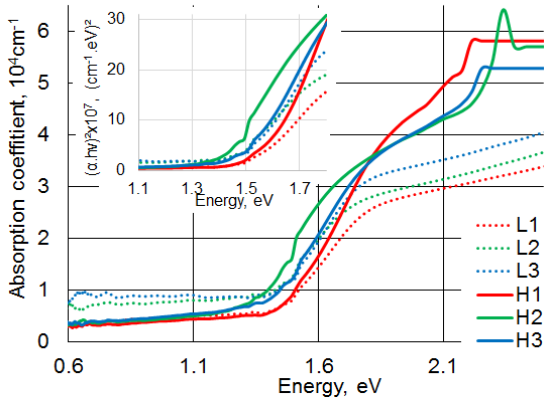

Figure 6: Absorption coefficients spectra and Tauc plots

The bandgap seems to be impacted by the Cu/Sn ratio and increases with increase of Sn concentration, while the absorption coefficient is almost constant (Fig. 7). This in accordance with published discussion about Cu/Sn ratio impact on bandgap [13].

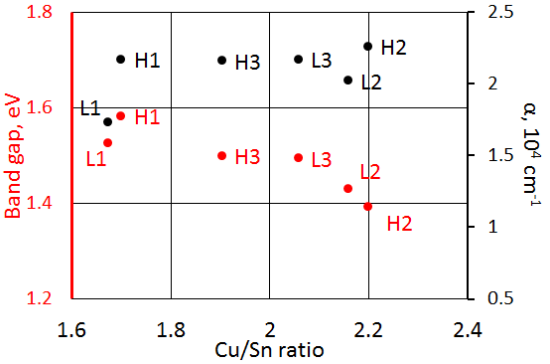

Figure 7: Optical properties versus Cu/Sn ratio.

Reported results of electrical properties widely vary among research groups and fabrication methods: carrier concentration (p) ranges from 10^{16} to 10^{19} cm^{-3}; hole mobility (μ_h) from 0.1 to 30 $cm^2V^{-1}s^{-1}$ and corresponding resistivity from 0.1 to 980 Ω.cm [14, 15, 16, 17].

Our Hall measurement results (Fig. 8, Table III) also present large range of electrical properties from low (10^{12} cm^{-3}) to high (10^{20} cm^{-3}) p-type carrier concentration, with a tendency to be inversely proportional to carrier concentration.

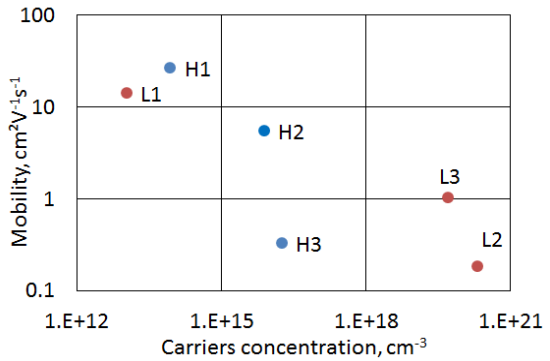

Figure 8: Hole mobility correlation with carrier density.

A linear increase of the carrier concentration with copper concentration in the samples has been observed, similarly to what was reported previously in [18]. Furthermore the mobility increases with tin concentration and the S/metal ratio, except for sample L1. This observation suggests that, for similar ranges of carrier concentration, such as H2 and H3 samples, the tin concentration influences on the mobility. Another possible explanation could be hidden in the unknown effect of sulfur atoms on the conduction mechanisms (Fig. 9).

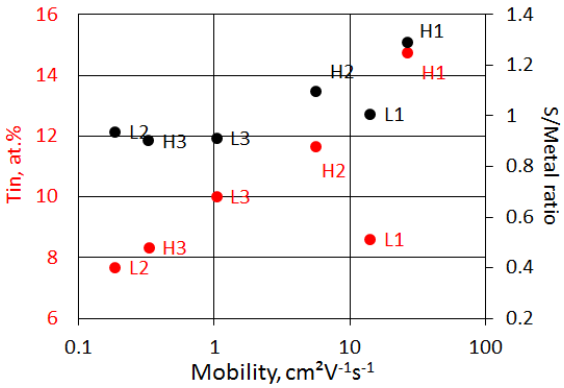

Figure 9: The correlations between mobility and tin or sulfur concentration.

3.3 Simulation optimization

According to SCAPS simulations (Fig. 10), samples H1 and H2 show the most suited p and μ_h values for higher PV efficiency. Note that simulations are limited to 10^{17} cm^{-3} doping levels, below which a rectifying behaviour is obtained, while higher doping levels tend to yield resistive behaviour as observed experimentally before.

The H2-based cell has been used for calibrating predictive SCAPS simulations. Under AM1.5 illumination, the measured photocurrent (I_{PH}) was about 12.7 mA/cm^2 after light soaking of 1.5 hour at negative bias, but extracted efficiency was extremely low (η = 0.78%). Such low cell performance can be related to the S-shape behaviour of J-V characteristics, indicating the presence of Schottky barrier at the rear contact - CZTS/Mo interface (estimated to be about 0.55 eV) and other resistances related problems, namely R_S=313 Ω.cm^2 and R_{SH}=157 Ω.cm^2.

Therefore, to estimate and predict the future roadmap of our H2-based cell process, we have excluded the impact of R_S and R_{SH} by changing their values to experimentally achievable ones [19]. This was followed by the optimization of the key intrinsic optoelectrical parameters such as μ_h, μ_e, p, E_G, α and barrier height. The baseline parameters used for the SCAPS simulations are provided in Table IV.

Impact of R_S, and R_{SH} : Firstly, we estimate the gain in cell efficiency when improving the R_S and R_{SH} from 313 Ω.cm^2 and 157 Ω.cm^2 (measured) to 4 Ω.cm^2 and 2000 Ω.cm^2 (optimization based on experimental values reported in the literature [19]) respectively. Using these values with the measured optoelectronic properties (Fig. 11) as inputs to the SCAPS simulator, a cell efficiency achieved of 3.63 % (i.e. a gain of 2.85 % abs compared to experimental values).

Impact of barrier height at CZTS/Mo interface : In the previous simulations, a barrier height of 0.55 eV have been considered. This level of barrier height at the rear contact is clearly detrimental for the solar cell performances (due to reduced V_{OC} and FF). Therefore, a barrier height of

0.27 eV at the CZTS/Mo interface is next considered. This yields an efficiency of 4.45 % (i.e. a 0.82 % abs gain). These gains in cell efficiencies might look marginal and not so important compared to other optoelectronic parameters. However, the impact of rear contact barrier height gets critically important while moving towards a fully optimized high-efficiency solar cell (where poor FF will significantly impact the cell efficiencies due to barrier height).

Impact of intrinsic μ_h and p : In Fig. 10, we can clearly appreciate the impact of μ_h and acceptor doping concentration (p) on cell efficiency. Therefore, in our SCAPS efficiency-optimization roadmap predictions, we next improve the μ_h from 5.52 $cm^2V^{-1}s^{-1}$ to 25 $cm^2V^{-1}s^{-1}$ and the acceptor concentration from p = 7.8×10^{15} cm^{-3} 5.5×10^{17} cm^{-3} (in all our simulations we have maintained the ratio of μ_h / μ_e to 4 for practicality). This leads to a simulated cell efficiency improvement from 4.45 % to 6.23 %.

Impact of CZTS bandgap (E_G) and absorption (α) : The extracted optical bandgap of H2 absorber is 1.39 eV. It is well known that larger bandgap materials contribute to better V_{OC} and cell efficiencies. Therefore, the next optimization parameter considered for higher cell efficiencies is improved E_G of 1.6 eV in the SCAPS simulations. This eventually led to an increment in the cell efficiency at 6.79 % (i.e. a 0.56 % abs gain). Next, in order to improve the photo-generated current (I_{PH}), it is important to have a higher absorption coefficient of the CZTS films. Therefore, we have increased the absorption coefficient from 2×10^4 cm^{-3} to 3.5×10^4 cm^{-3} in our simulations. This resulted in an improved cell efficiency of 8.44 % (1.65 % abs gain).

Lastly, further optimization of deep defect concentrations (N_{def}) by an order or magnitude (i.e. from 2×10^{18} cm^{-3} to 2×10^{17} cm^{-3}) yields a further improvement in cell efficiencies to 9.27%.

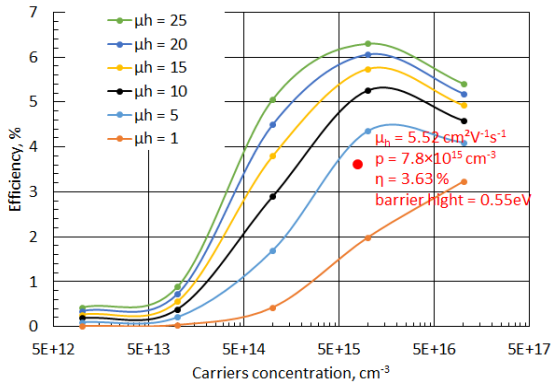

Figure 10: SCAPS simulation efficiency prediction for different hole mobilities (μ_h), carrier concentrations using input parameters from fig. 11 but after optimizing R_S, R_{SH} and barrier height. The red dot corresponds to our experimental cell measurement after R_S and R_{SH} corrections

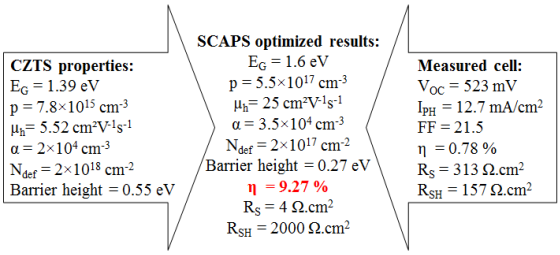

Figure 11: Experimental inputs from material and cell characterizations (left and right) and SCAPS optimization results (middle)

Table IV: Baseline parameters used for modelling CZTS solar cells

Parameter	CZTS	CdS	i-ZnO	ZnO:Al
E_g (eV)	1.39	2.4	3.3	3.3
χ (eV)	4.5	4.45	4.55	4.55
$\varepsilon/\varepsilon_0$	13.6	10	9	9
N_c (cm^{-3})	2.2×10^{18}	1.3×10^{18}	3.1×10^{18}	3×10^{18}
N_v (cm^{-3})	1.5×10^{19}	9.1×10^{18}	1.8×10^{19}	1.8×10^{19}
V_e (cm/s)	3.9×10^{7}	3.1×10^{7}	2.4×10^{7}	2.4×10^{7}
V_h (cm/s)	1.4×10^{7}	1.6×10^{7}	1.3×10^{7}	1.3×10^{7}
μ_e (cm^2/Vs)	4*μh	72	100	100
μ_h (cm^2/Vs)	5.52	20	31	3
Doping (cm^{-3})	7.8×10^{15} (a)	5×10^{17} (d)	1×10^{17} (d)	5×10^{19} (d)
	Bulk defect properties			
N (cm^{-2})	10^{14} (D)	5×10^{16} (A)	10^{16} (A)	10^{16} (A)
σ_e (cm^2)	10^{-15}	10^{-15}	10^{-15}	10^{-15}
σ_h (cm^2)	10^{-11}	5×10^{-13}	5×10^{-13}	5×10^{-13}

(a) and (d) denote shallow acceptor and donor defect while (A), (D) and (N) denote deep acceptor, donor and neutral defects.
Nomenclature: ΔE_c: Conduction and band offset; E_g: Band gap; $\varepsilon/\varepsilon_0$: Relative permittivity; χ: Affinity; μ_e, μ_h: Velocity of electrons and holes; N_c, N_v: Effective density of states in conduction and valence bands; σ_e, σ_h: Capture cross-section of electrons and holes

4 CONCLUSION

Two groups of metallic precursors have been studied by sequential sputtering, i.e. low- and high-density layers varying composition ratios and/or stack ordering, and finalized into CZTS absorber layers by RTP with presence of S. For all samples material and electrical characterizations have been performed. No significant difference has been observed by XRD and Raman in the crystal structures of the two groups. They all exhibit rough surface with different textures and mainly CZTS phase, coexisting with CTS, $Cu_{2-x}S$ and ZnS phases. From optical characterization, the bandgap energies and absorption coefficients vary respectively from 1.39 to 1.58eV and from 1.73×10^4 to 2.26×10^4 cm^{-1}, suitable for solar cell application and the correlation of the bandgap energy with

Cu/Sn ratio is observed. Carrier concentration and mobility Hall measurements show clear correlations with Cu and Sn concentrations in CZTS layers respectively.

With the measured CZTS optoelectronic properties of H2-based cells as starting inputs to the SCAPS simulator, we have clearly distinguished the impact of each key optoelectronic parameter. Improving these optoelectronic properties, beyond the absorber composition and morphology, is key to achieve above 10%-efficiency CZTS cells. Monitoring of these optoelectrical parameters during the fabrication steps could then be particularly relevant to assess the absorber quality in industrial process.

5 ACKNOWLEDGEMENTS

Authors are grateful to Edgardo Saucedo (IREC, Barcelona) and his team for sharing their experience and valuable advice for this work. We are thankful to Walloon Region and FNRS for financial support. Thanks to Sergio Bernardi for valuable discussions and Ferran Urena Begara for help in Raman interpretation.

6 REFERENCES

[1] K. Sun, et al, Over 9% efficient kesterite Cu2ZnSnS4 solar cell fabricated by using Zn1-XCdXS buffer layer, Adv. Energy Mater. 6 (2016) 1600046-1600052

[2] A. Fairbrother, et al, Development of selective chemical etch to improve the conversion efficiency of Zn-rich Cu2ZnSnS4 solar cells. J. Am. Chem. Soc. 134 (2012) 8018-8021

[3] A.A. Rockett, et al, Current status and opportunities in chalcopyrite solar cells, Curr. Opin. Solid State Mater. Sci. 14 (2010) 143–148

[4] R. Liu, et al, Preparation of high-quality Cu2ZnSnS4 thin films for solar cells via the improvement of sulfur partial pressure using a static annealing sulfurization approach, Sol. Energy Mater. Sol. Cells 157 (2016) 221-228

[5] C. Yan, et al, Boost Voc of pure sulfide kesterite solar cell via a double CZTS layer stacks, Sol. Energy Mater. Sol. Cells 160 (2017) 7-11

[6] Y. Ren, et al, Influence of the Cu2ZnSnS4 absorber thickness on thin film solar cells, Phys. Status Solidi A 212, (2015) 2889-2896

[7] S.M. Pawar, et al, Synthesis of Cu2ZnSnS4 (CZTS) absorber by rapid thermal processing (RTP) sulfurization of stacked metallic precursor films for solar cell application. Mater. Lett. 118 (2014) 76-79

[8] https://www.webelements.com/periodicity/density/

[9] S. Lopez-Martino, et al, Earth-abundant absorber based solar cells onto low weight stainless steel substrate. Sol. Energy Mater. Sol. Celles 130 (2014) 327-353

[10] M. Patel, et al, Enhancement of output performance of Cu2ZnSnS4 thin film solar cells – A numerical simulation approach and comparison to experiments, Physica B 407 (2012) 4391-4397

[11] P.-A. Cormier, et al, One-step synthesis of Cu2ZnSnS4 thin films by reactive magnetron co-sputtering. Acta Materialia 96 (2015) 80-88

[12] K. Ito, et al, Electrical properties of stannite type quaternary semiconductor thin films. Jap. J. of Applied Phys. 27-11 (1988) 2094-2097

[13] C. Malerbe, et al. CTZS stoichiometry effects on the band gap energy. J. of Alloys and Compounds 582 (2014) 528-534

[14] Z. Shi, et al, Kesterite-based next generation high performance thin film solar cell: current progress and future prospects, J. Mater. Sci: Mater Electron 28 (2017) 2290-2306

[15] O. Vigil-Galán, et al, Electrical properties of sprayed Cu2ZnSnS4 thin films and its relation with secondary phase formation and solar cell performance. Sol. Energy Mater. Sol. Cells 132 (2015) 557-562

[16] J.C. Gonzalez, et al, Influence of the sulfurization time on the morphological, chemical, structural and electrical properties of Cu2ZnSnS4 polycrystalline thin films, Sol. Energy Mater. Sol. Cells 123 (2014) 58-64

[17] F. Liu, et al, Insitu growth of Cu2ZnSnS4 thin films by reactive magnetron co-sputtering, Sol. Energy Mater. Sol. Cells 94 (2010) 2231-2434

[18] E.M. Mkawi, et al. Dependence of copper concentration on the properties of the Cu2ZnSnS4 thin films prepared by electrochemical method. Int. J. Electrochim. Sci. 8 (2013) 359-368

[19] W. Wang, et al, Device characteristics of CZTSSe thin-film solar cells with 12.6% efficiency. Adv. Eng. Mater. 4-7 (2014)